

Al-Ag alloy formation by aluminium underpotential deposition from $\text{AlCl}_3 + \text{NaCl}$ melts on silver substrate

B. S. Radović¹, R. A. H. Edwards¹, V. S. Cvetković², J. N. Jovičević^{2*}

¹*Institute for Advanced Materials, Joint Research Centre, I 21020 Ispra, Italy*

²*Faculty of Sciences and Mathematics, University of Priština, 38220 K. Mitrovica, Serbia*

Received 19 March 2009, received in revised form 21 September 2009, accepted 23 September 2009

Abstract

Aluminium was incorporated into silver electrodes by underpotential deposition from an equimolar $\text{AlCl}_3 + \text{NaCl}$ melt at 200 °C, 250 °C and 300 °C. The process was studied by linear sweep voltammetry and potentiostatic deposition/galvanostatic stripping. The deposits were characterized by electron probe and glancing incidence X-ray diffraction. The electrochemical measurements showed clear evidence of formation of two intermetallic compounds. This was confirmed by the analysis, which showed two layers of successive bulk intermetallic compounds. The Gibbs energy of formation of the compounds is calculated and the kinetics of growth is described.

Key words: aluminium-silver alloys, underpotential deposition, diffusion, microscopy and microanalysis techniques, Gibbs energy of formation, kinetics

1. Introduction

One of the ways to obtain metals and metal alloys is the direct isothermal electrodeposition. In addition, the deposition current density provides direct measure of the deposition rate. Electrodeposition of metals and alloys is essential for a variety of industries including electronics, optics, sensors, automotive and aerospace, to name but a few. The electroplating industry, which dates back well over 100 years, is based solely on aqueous solutions due to the high solubility of electrolytes and metal salts resulting in highly conducting solutions. Electrodeposition of metals and alloys from solutions has been extensively elaborated in [1–4].

However, neither aluminium nor its alloys can be electrodeposited from aqueous solutions, because hydrogen is evolved before aluminium is plated. Aluminium and its alloys are important materials for the fabrication of corrosion-resistant, lightweight, high-strength structures. It has been demonstrated that the corrosion resistance of aluminium can be significantly improved by alloying it with transition metals such as Cr, Cu, Mo, Mn, Nb, Ta, Ti, V, Zn, and Zr. On the other hand, small additions of aluminium can

also significantly improve properties of other metals. For example, aluminium bronze is a strong corrosion-resistant alloy of copper, and small amounts of aluminium added to nickel provide strengthening of the nickel-based superalloys [5]. The desire to electrodeposit metals and their alloys such as Al, Ti and W was the main driving force for non-aqueous electrolytes.

Among the non-aqueous solvents that have been used successfully to electrodeposit metals and their alloys [6–9], as well as aluminium and its metal alloys [10, 11], are the chloroaluminate molten salts [12, 13], which contain inorganic [12–17] or organic [12, 18–21] chloride salts combined with anhydrous aluminium chloride. The chloroaluminate molten salts seem to be ideal solvents for the electrodeposition of metal-aluminium alloys, because they constitute a reservoir of reducible aluminium-containing species, they are excellent solvents for many metal ions, and they exhibit good intrinsic ionic conductivity [12, 13, 19–22].

Detailed exploration of metal electrodeposition processes led to the recognition of underpotential deposition (UPD) – the deposition of metals on foreign metal substrate at electrode potentials more positive than the Nernst-potential of the corresponding three-dimensional deposited metal bulk phase [23, 24]. In

*Corresponding author: tel.: ++381 063 343140; fax: ++381 25 425398; e-mail address: matori47@hotmail.com

solutions, it has been a subject of research for more than fifty years [23–30]. Soon, the phenomenon of UPD from melts [12, 20, 31, 32] was also recognized, and it was well documented in the case of aluminium UPD from inorganic [12, 14, 33, 34] and organic melts (ionic liquids) [7, 12, 35–37].

Work on UPD of metals from solutions revealed that a metal, electrodeposited onto a metal cathode into which it can diffuse at room temperature, makes a surface alloy with the substrate [38–43]. This was also realized for aluminium UPD from inorganic [12, 14, 33, 38–47] and organic melts [12, 37, 48, 49].

Knowledge and experimental experience accumulated on UPD lead to alloy formation by UPD codeposition from solutions [4, 50–52]. As the name suggests, the method consists of codepositing at least two elements from the same solution. The same was found to be true for some alloys [32, 44] and aluminium alloys from inorganic [12] and organic melts [12, 44–46].

Electrodeposited alloys may differ considerably in their chemical and phase constitution from alloys of the same chemical composition but obtained by metallurgical (thermal) methods. Many examples are reported in the literature with some controversy on the phases obtained and their composition limits. The problem was examined in the past [1, 2], and more recently [12], showing some important cases of UPD alloys with phase structure differing from that of metallurgical alloys.

UPD of metals [25–29] from solutions and formation of alloys by UPD of aluminium from inorganic melts onto surface of different metals [14, 33, 34] have been a subject of our work for more than twenty years. Initially, we observed aluminium UPD from $\text{AlCl}_3 + \text{NaCl}$ melt on several metal electrodes [14] inducing surface alloy formation. Our more elaborate study of aluminium UPD on Au revealed formation of four Au-Al alloys formed by diffusion of underpotentially deposited aluminium into gold substrate [33, 34]. Others obtained similar results on gold (111) oriented single crystal [37] and on polycrystalline gold [53] from organic melts. The differences observed, most probably result from the difference in the deposition temperatures. Working temperatures in organic chloroaluminate melts range between 20°C and 100°C, while in inorganic melts working temperatures start well above these. It has been shown that temperature influences thermodynamics and kinetics of UPD of metals [26]. Higher temperatures promote reaction between the substrate and the depositing element, and solid-state interdiffusion dependence on temperature is also well known. The differences in anions present in the electrolytes used are of some importance, too [27, 28, 54, 55].

There are no records of aluminium UPD on silver from melts in literature, although there are examples of codeposition of Ag-Al alloys at the potentials more

positive than the bulk Al equilibrium potential on platinum and tungsten [12, 46] from ionic liquids.

In the present study, the UPD of aluminium on polycrystalline substrate of silver from $\text{AlCl}_3 + \text{NaCl}$ equimolar melts was investigated by electrochemical techniques and surface analysis. The data on the influence of temperature and deposition time were correlated with the analysis results to produce data describing the thermodynamics and kinetics of the formation of several intermetallic compounds.

2. Experimental details

2.1. Electrochemical experiments

All electrochemical experiments were carried out in an electrochemical cell designed for work with melts, under a purified argon atmosphere [13, 22]. The cell was made of Pyrex glass and placed in a furnace.

Aluminium wire 3 mm in diameter (99.999 % pure, Alfa Products, Thiokol/Ventron division, USA) was used as a reference electrode in a Luggin capillary whose tip was placed close to the working electrode. This was to minimize the error in the measured potential associated to IR drop in the melt between the tip of the Luggin capillary and the working electrode. An aluminium plate (99.999 % pure, Alfa Products, Thiokol/Ventron division, USA) was used as a counter electrode. Two types and sizes of working electrodes were used. The one for electrochemical experiments consisted of 1 mm diameter 99.99 % pure silver wire pressed into a glass tube of slightly larger diameter such that only 1 cm² area of the metal wire was exposed to the melt. The other was 2 cm² 99.99 % pure silver plate working electrode for surface/sub-surface analysis. It was clipped (above the melt surface) onto a conductive wire pressed into a glass tube.

The aluminium reference and counter electrodes were first mechanically polished consecutively on emery papers of grade 0, 00, 000, and 0000, and then on polishing cloths (“Buhler Ltd.”) impregnated with alumina (“Banner Scientific Ltd.”) of 1 μm, 0.3 μm and 0.05 μm grades. After undergoing mechanical polishing procedure, the aluminium reference and counter electrodes were subsequently etched in solutions of 50 vol.% HF + 15 vol.% H₂O and conc. NH₄OH + 5 vol.% H₂O₂ prior to each experiment. All glassware was washed with triple distilled water and alcohol and dried at 120°C for at least one hour prior to use.

The working electrodes for electrochemical experiments were mechanically polished and before introduction into the process each silver-working electrode was chemically polished. The electrode was immersed into the mixture of solutions (20 g l⁻¹ NaCN : 20 vol.% H₂O₂ = 1 : 1) for 5–10 s and intensely stirred, then exposed to air for 20–30 s, returned for 1 s to the

mixture of solutions, followed by holding it in the water solution with 37.5 g l^{-1} NaCN until gas bubbles on the electrode surface stopped evolving. The electrode was then washed with triply distilled water.

The working electrodes-samples for surface/sub-surface analysis were mechanically polished with emery papers. Initially the largest grade was used and then progressively smaller ones down to the 0000 on emery paper, until the electrode had a mirror-like appearance free from scratches or blemishes. All mechanical polishing steps were always performed manually rather than on a polishing machine, which was less convenient to use. The electrode was then chemically etched as described above.

Examination of the electrode surface under the optical microscope and with X-ray emission spectroscopy revealed no contaminating elements.

Sodium chloride (NaCl p.a., “Merck”) and aluminium (III) chloride (99.99 % pure AlCl_3 , “Aldrich Chemical Company, Inc.”) were used for melt preparation.

Since aluminium (III) chloride is extremely sensitive to moisture and oxygen, special attention was paid to the chemicals and to the melt preparation. The sodium chloride was reduced to fine powder, dried in a furnace at 500°C for five hours and kept in vacuum at 120°C until use, in order to remove bonded water. This procedure was counter-productive for drying aluminium (III) chloride, which absorbs water irreversibly during any handling. Therefore no drying procedure was applied; instead, fresh, sealed bottle of anhydrous AlCl_3 was used for each experiment. The procedure of melting the $\text{AlCl}_3 + \text{NaCl}$ mixture consisted of heating (in inert atmosphere) a vessel with AlCl_3 , at the bottom and NaCl on top at 250°C , where upon all the AlCl_3 sublimed forming a homogeneous $\text{AlCl}_3 + \text{NaCl}$ melt by reaction with NaCl. The melt was subjected to pre-electrolysis between two aluminium (99.999 % pure) plates with large surface area (20 cm^2 each) at $220\text{--}250^\circ\text{C}$ with constant current density $i = 1.5 \times 10^{-2} \text{ A cm}^{-2}$ for 10 h. Both aluminium plates were cleaned before use, in the same way as the reference electrode. After the pre-electrolysis, linear sweep voltammogram performed on vitreous carbon cathode in the melt showed only double layer charging and discharging features in the potential region between $0.005\text{--}1.85 \text{ V vs. Al}$.

Two different electrochemical techniques were used in the experiments: linear sweep voltammetry (LSV) and potentiostatic UPD followed by galvanostatic stripping. Two different procedures of LSV were carried out one after the other, as follows:

a) The potential range was scanned from a potential $0.050\text{--}0.100 \text{ V}$ negative to the open circuit potential of the silver electrode ($0.8\text{--}0.850 \text{ V}$ measured against the aluminium reference electrode) to a potential $0.010\text{--}0.150 \text{ V}$ positive to the reversible aluminium

potential, followed by the return scan. The sweep rate was 0.010 V s^{-1} ;

b) Then the same potential range was scanned except that the scan was interrupted when the potential reached $0.010\text{--}0.150 \text{ V}$ positive to the reversible aluminium potential, and this potential was held for $\tau_d = 1, 3, 6, 9,$ and 15 min before starting the return scan. The sweep rate was as in a).

The procedure for the potentiostatic UPD followed by galvanostatic stripping was as follows:

a) The specimen was held at $0.050\text{--}0.100 \text{ V}$ negative to the open circuit potential of silver ($0.8\text{--}0.850 \text{ V vs. Al}$) to strip any aluminium already deposited. Then the potential was stepped to the $0.010\text{--}0.150 \text{ V}$ from the reversible potential of aluminium;

b) This potential ($E_d = 0.010\text{--}0.150 \text{ V vs. Al}$) was maintained for $\tau_d = 1, 3, 6, 9, 15 \text{ min}$, after which the potential was switched out of circuit to open the electrode circuit. The electrode potential was then recorded by an XY recorder as a function of time, whilst a small current ($\cong 0.02 \text{ mA cm}^{-2}$) slowly stripped the aluminium from the surface silver specimen. If the stripping current was interrupted for a few seconds, the measured potential did not change detectably. This shows that the activation overpotential caused by the stripping current was negligible and the potentials measured can be considered open circuit potentials.

All electrochemical measurements were carried out using a Universal programmer (PAR-M175), a potentiostat (PAR-M173) and an X-Y-t recorder (Hewlett Packard M7040A). The temperature of the melt was monitored by a chromel-alumel thermocouple with an accuracy of 1°C .

2.2. Surface/sub-surface analysis

Glancing incidence X-ray diffraction (GIXRD) and electron microprobe analysis (EPMA) of polished cross-sections were used as techniques for surface/sub-surface analysis. These techniques were applied comparatively to blank probes polished mechanically and chemically and samples after electrochemical UPD. Sample preparation for the surface/sub-surface analysis was as follows: aluminium was electrodeposited from the equimolar $\text{AlCl}_3 + \text{NaCl}$ melt at constant underpotential ($E_d = 0.010\text{--}0.150 \text{ V vs. Al}$) for different periods of time ($\tau_d = 1, 2$ and 4 h) at three different temperatures ($t = 200^\circ\text{C}, 250^\circ\text{C}$ and 300°C). Deposition was started 5 min after insertion of the working electrode in order to allow thermal equilibrium. The working electrode was then removed from the melt whilst still under polarization, then washed repeatedly under distilled water, air dried and stored in a desiccator until use.

The crystallographic structure present near the surface of these specimens was determined using glancing angle X-ray diffraction at an incident angle of

Table 1. Peak potentials E (V vs. Al) and the corresponding anodic current densities i (10^{-3} A cm^{-2}) observed in the anodic part of linear sweep voltammograms on silver electrodes as a function of deposition time τ_d (s) and temperature t ($^{\circ}\text{C}$)

τ_d (s)	0		60		180		360		540	
t ($^{\circ}\text{C}$)	E	i	E	i	E	i	E	i	E	i
200	0.25	0.23	0.25	0.42	0.3	0.78	0.33	1.28	0.34	1.71
	0.68	0.31	0.7	0.43	0.69	0.73	0.7	1.39	0.71	1.65
250	0.1	0.64	0.2	4.48	0.22	6.96	0.25	8.96	0.27	10.1
	0.69	0.32	0.7	0.8	0.7	1.68	0.71	3.04	0.73	4.32
300	0.13	0.81	0.16	10.5	0.15	11.1	0.21	12.9	0.21	13.1
	0.67	0.09	0.067	0.52	0.7	1.4	0.7	6.1	0.71	7.8

Table 2. Total anodic dissolution charges (mC cm^{-2}) and mass (10^{-6} g cm^{-2}) calculated of Al deposited as a function of deposition time, τ_d (s), and temperature, t ($^{\circ}\text{C}$), for silver electrodes (LSV experiments)

t ($^{\circ}\text{C}$)	τ_d (s)	0	60	180	360	540
200	Total anodic charge	0.9	8.82	11.5	18.5	24.5
	Mass of Al deposited	0.08	0.83	1.08	1.74	2.3
250	Total anodic charge	5.8	85.7	173	253.8	307
	Mass of Al deposited	0.54	8.06	16.26	23.86	28.86
300	Total anodic charge	11	142	241.2	339	405.6
	Mass of Al deposited	1.03	13.35	22.68	31.87	38.13

Table 3. Average plateau potential values E (V vs. Al) obtained in “open circuit” measurements of aluminium deposited on silver at different times τ_d (s) and various temperatures t ($^{\circ}\text{C}$) (see Fig. 2)

t ($^{\circ}\text{C}$)		200			250			300		
τ_d (s)		60	180	540	60	180	540	60	180	540
Plateau potential	E_1	0.08	0.09	0.11	0.11	0.11	0.12	0.11	0.1	0.11
V vs. Al	E_2	0.63	0.63	0.64	0.62	0.64	0.64	0.62	0.61	0.62

1° to the surface. A multipurpose glancing angle X-ray spectrometer using a standard X-ray tube and germanium solid state detector was used. The spectrometer was controlled by an IBM-PC-XT computer with Superior electric microstepping motors powering various goniometer motions. The detector pulses were timed and counted using a Tecmar Lambaster interface.

To prepare cross-sections for EPMA examination, samples, which had been used as working electrodes were first cut into smaller plates, typically 1/3 of the original size. These were supported vertically in clips and covered with conductive plastic powder. The sample in powder was then pressed into a disc (2.5 cm diameter and 1 cm height) and the remaining visible edge of the sample polished to 0.1 mm. EPMA was carried out using a CAMEBAX-R electron microprobe.

3. Results

Examples of the linear sweep voltammograms for aluminium underpotential deposition on silver electrodes at different deposition times (τ_d) and at various temperatures (t) are shown in Fig. 1. The potential values E (V vs. Al) and the corresponding current densities i (10^{-3} A cm^{-2}) for the dissolution peaks observed in the anodic parts of the voltammograms as a function of the deposition time τ_d and temperature t are summarized in Table 1. The total anodic dissolution charge $Q_{\text{Al,max}}$ and calculated mass of aluminium deposited on silver electrodes, as a function of the deposition time and temperature, are listed in Table 2. $Q_{\text{Al,max}}$ values were obtained by integration of the linear sweep voltammograms to give the surface area bounded by the anodic current and the horizontal axis. The values E , i_p and $Q_{\text{Al,max}}$ presented

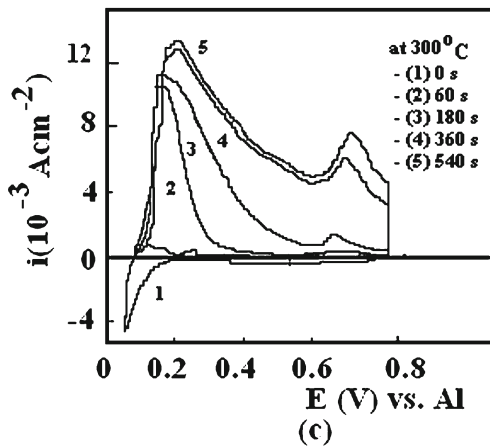
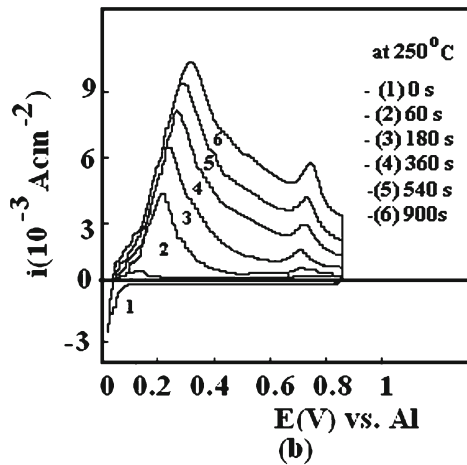
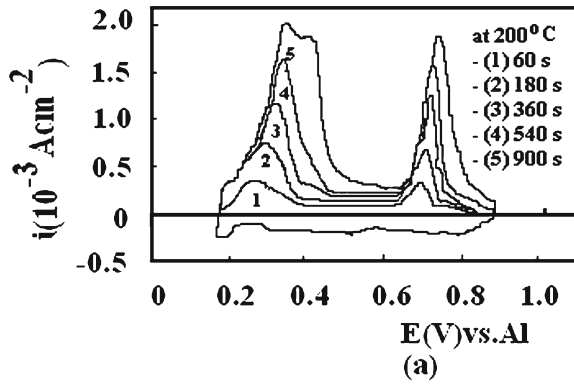


Fig. 1. Linear sweep voltammograms of aluminium dissolution from the silver electrode obtained with a sweep rate 10 mV s^{-1} : (a) at 200°C , (b) at 250°C , (c) at 300°C .

in Tables 1 and 2 are average values obtained from five or more measurements. The mass of aluminium deposited was calculated from Faraday's law.

Representatives of the potential/time diagrams of aluminium dissolution from silver electrodes, obtained by low-current galvanostatic stripping ("open circuit measurements") following UPD of various times and

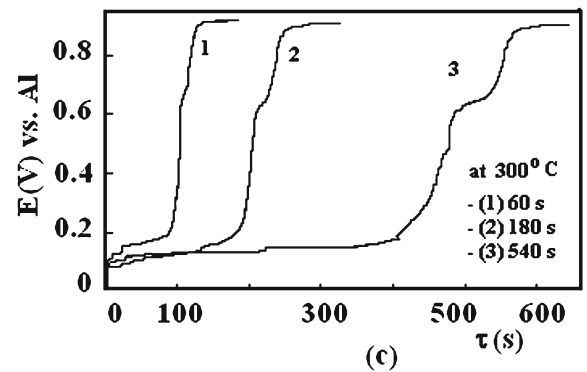
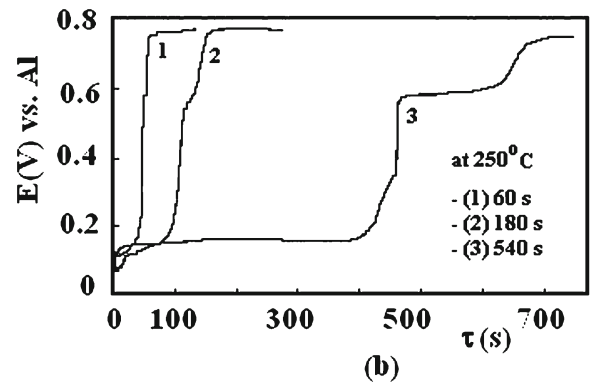
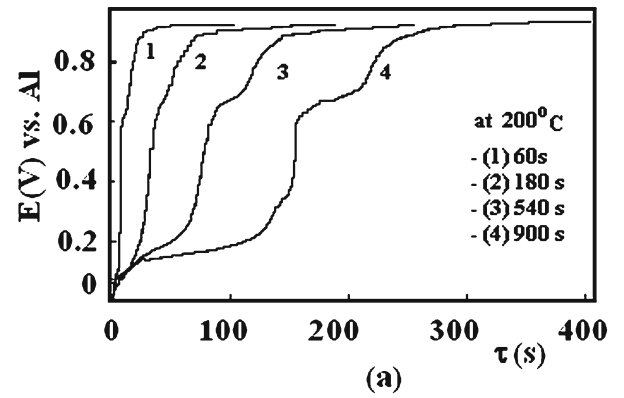


Fig. 2. "Open circuit" graphs of aluminium dissolution after UPD of aluminium on silver electrode: (a) at 200°C , (b) at 250°C , (c) at 300°C .

different temperatures, is given in Fig. 2. Table 3 summarizes the average potential values at the observed plateaux for five or more measurements.

An example of the diffraction patterns taken of the silver samples after aluminium underpotential deposition as a function of temperature and deposition time is given in Fig. 3. The phases and their crystallographic systems identified in the deposits obtained are listed in Table 4. The phases were identified using JCPDS files [56–58] and the reference for each phase is also supplied.

Examples of the depth profiles of aluminium into

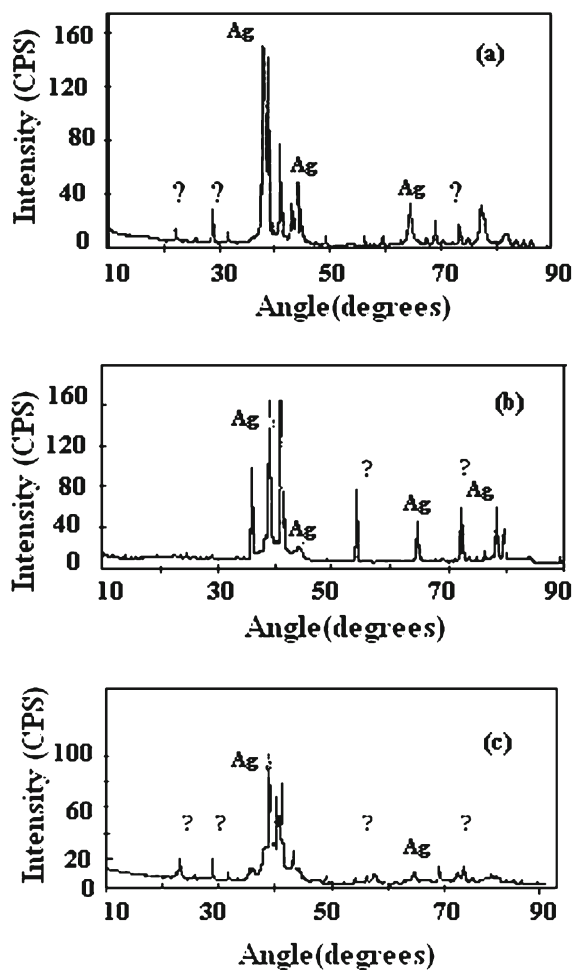


Fig. 3. Diffraction patterns of the silver samples after: (a) one hour, (b) two hours, (c) four hours of aluminium underpotential deposition at 250°C.

silver, as a function of temperature and deposition time (obtained by electron-probe microanalysis), are given in Fig. 4 and summarized in Table 5.

EPMA maps of aluminium distribution at the edge of silver samples after two hours of aluminium underpotential deposition at 200°C and 300°C are shown in Fig. 5.

4. Discussion

4.1. Linear sweep voltammograms: influence of deposition time and temperature

The reversible potential of silver was more positive than the reversible potential of aluminium in the same system. This allowed a wide potential range, anodic to the aluminium reversible potential, i.e. the aluminium underpotential deposition region, to be studied.

In general, the fine structure of the cathodic cur-

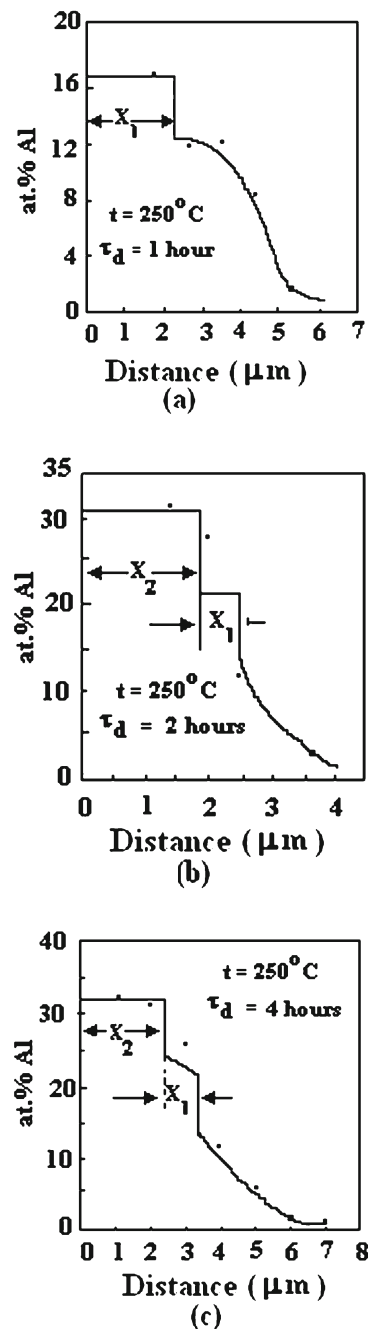


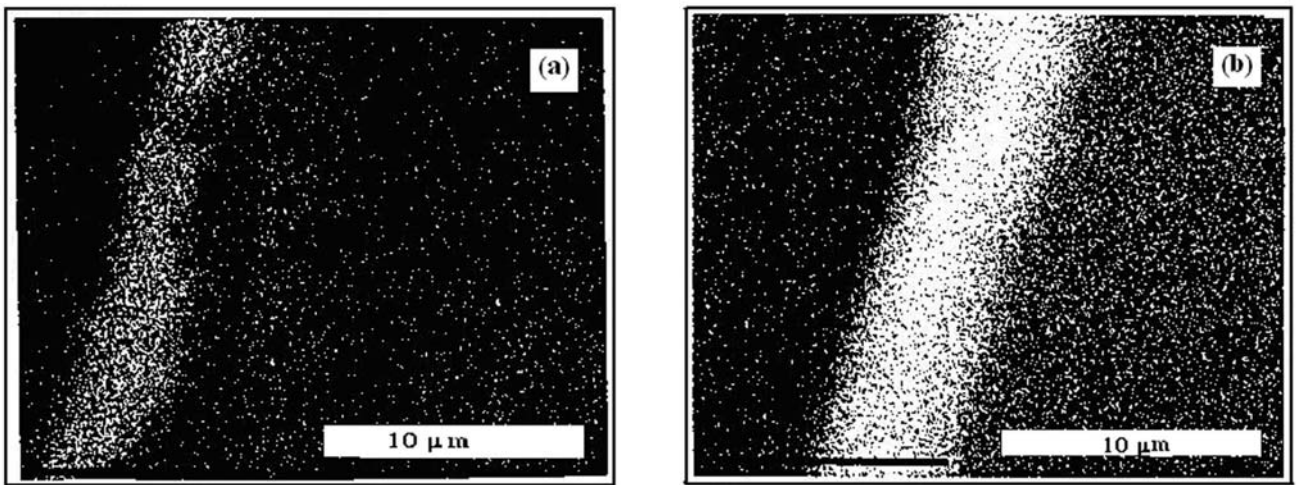
Fig. 4. Depth profile of aluminium into the silver sample obtained after: (a) one, (b) two and (c) four hours of aluminium underpotential deposition at 250°C.

rent peaks of linear sweep voltammograms was less pronounced than the anodic one. The anodic current peaks were more readily defined, particularly in the case of a prolonged underpotential deposition.

Ideally, one should record the potential at the beginning of corresponding anodic and cathodic peaks. Instead, in this case the current peak potential values were measured between peak valleys values. This was done for two reasons:

Table 4. The phases identified on silver samples after aluminium underpotential deposition at different times and various temperatures together with their crystallographic systems and references (see Figs. 1 and 2)

t (°C)	τ_d (h)	Identified phase	Crystallographic system	Reference
200	2	–	–	–
250	1	Ag ₃ Al	cubic	[57]
	2	Ag ₃ Al	cubic	[57]
		Ag ₂ Al	hexagonal	[57]
	4	Ag ₃ Al	cubic	[57]
Ag ₂ Al		hexagonal	[58]	
300	2	Ag ₂ Al	hexagonal	[58]

Fig. 5. Al K α emission map at the edge of the silver sample obtained after two hours of aluminium underpotential deposition at: (a) 250°C and (b) 300°C (marker 10 μm).Table 5. The depths (μm) of the formed layers (x_1 and x_2) on silver samples after aluminium underpotential deposition at different times τ_d (h) and different temperatures t (°C) obtained by EPMA (* due to technical error during the treatment of the melt no meaningful data could be obtained from the subsequent analysis)

t (°C)	τ_d (h)	x_1 (μm)	x_2 (μm)
200	2	*	*
250	1	2.3	–
	2	0.65	1.65
		4	1
300	2	2.08	2.69

– cathodic peak separation was not as well pronounced as in the case of single crystal substrates [37–42, 48, 49], which prevented exact cathodic to anodic peak attribution;

– anodic current peaks were well merged thus preventing exact allocation of the peak starting potential.

In general, the total recorded charges bounded by the cathodic and anodic currents were similar (within $\pm 5\%$ difference) and symmetrical to the zero current axis.

The charge calculated for cathodic and anodic parts of the linear sweep voltammograms obtained, was significantly different from the charge needed for the deposition of the closest packed aluminium monolayer (Al atomic radius being 1.18×10^{-10} m) we calculated to be 1.17 mC cm^{-2} .

When the chosen cathodic end potentials, E_d , were maintained for longer times during linear sweep experiments, the cathodic current increase was not observed. This would suggest that the aluminium underpotential deposition after at least one aluminium monolayer completion proceeds at the rate necessary to compensate for the amount lacking of one aluminium monolayer, which entered solid-state intermetallic reaction with the substrate – silver. This dy-

dynamic quasi-equilibrium would seem to be maintained as long as intermetallic solid-state reaction proceeded by diffusion of aluminium into the substrate. Different anodic dissolution peaks would then reflect different intermetallic compounds formed during previous aluminium deposition, having naturally different dissolution potentials (Fig. 1).

When the holding (the deposition time, τ_d) of the silver electrode at the cathodic end potential, E_d , was increased, two characteristics of the anodic current peaks could be observed:

- anodic peak current values, i_p , increased with the cathodic end potential holding time τ_d ;
- the integrated charge under each of the anodic peaks (as well as the total anodic charge, $Q_{Al,max}$) increased proportionally to the square root of the cathodic end potential holding time $\tau_d^{1/2}$ (see Tables 1, 2 and Fig. 14).

It should be noted that the increase in working temperature of the system, all other conditions being kept the same, led to an increase of the charge under both cathodic and anodic peaks. Also, as it can be seen in Table 1, the anodic peak current values increased with increasing working temperature.

LSV data obtained strongly suggest that, under the given conditions, underpotentially deposited aluminium diffuses into silver substrate forming surface alloys.

4.2. Low-current galvanostatic stripping

To obtain the dissolution characteristics of the underpotentially deposited aluminium onto and into the silver substrate, the potential pulse with amplitude cathodically exceeding the potentials characteristic for the appearance of anodic peaks ($E_d = 0.010\text{--}0.150$ V vs. Al) was followed by a quasi-open circuit measurement of the electrode potential with time. The small constant dissolution current applied in the “open circuit” measurements resulted in the potential-time curves exhibiting plateaux brought about by dissolution material being able to sustain an equilibrium potential (or corrosion potential) with $AlCl_4^-$ in the melt, Fig. 2. The number of plateaux (Table 3) can be seen to agree with the number of anodic peaks obtained during the linear sweep measurements (Table 1). The potentials of the two plateaux in Fig. 2 correspond reasonably well to the potentials of the anodic current peaks in the LSV's. The existence of peaks in the linear sweep voltammograms indicates that these potentials are indeed reversible potentials (irreversible potential contributions such as activation overpotentials or diffusion overpotentials would increase monotonically with overpotential and not result in peaks).

In fact, when the cathodic pulse amplitude applied was more negative than the potential of the most anodic peak observed on the linear sweep voltammo-

gram, the plateau at the potential similar to the linear sweep voltammogram peak potential was recorded in the potential-time of curve of the “open circuit” measurement. When potential pulse amplitude exceeded both linear sweep voltammogram peak potentials, the potential-time curves of the “open circuit” showed two plateaux at the potentials very close to the voltammogram peak potentials. This allowed the charge belonging to each of the plateaux (aluminium-silver intermetallic compounds) produced during potential step to be calculated on the basis of the time it took to be dissolved (dissolution current density being constant at 0.02 mA cm^{-2}). The charges of cathodic deposition processes corresponded well to the anodic dissolution charges (within $\pm 3\%$) calculated as the multiple of dissolution current density and the time elapsed for the dissolution. Comparison of the charges obtained this way agreed very well (within $\pm 5\%$) with the charges under the anodic peaks limited by the same potential range in the LSV voltammetry.

Prolonged potentiostatic underpotential deposition brought about a proportional increase in the “open circuit” dissolution time, but this had little effect on the potentials of the plateaux. An increase in the working temperature, however, increased the amount of aluminium deposited and dissolved. This is again consistent with the previously described linear sweep voltammetry results.

The “open circuit” measurements, and particularly:

- a) the existence of the reversible (or corrosion) potential (two of them apart from reversible potential of silver substrate),
- b) the temperature dependence of these potentials,
- c) very similar behaviour of these potentials and the reversible aluminium potential,

gave strong support to the assumptions already made earlier, that intermetallic compounds are formed between silver substrate and underpotentially deposited aluminium.

4.3. Alloy formation

Both the linear sweep voltammograms of aluminium deposition/dissolution (Fig. 1) and low-current galvanostatic stripping measurements (Fig. 2) clearly show that some interaction between the substrate and aluminium from the melt occurs at a potential positive to the potential of the aluminium reference electrode. If there were a nucleation barrier for alloy formation, one would expect an increase in the cathodic current during holding at the cathodic-end potential. No such increase was observed, indicating dynamic quasi-equilibrium is maintained at the surface by diffusion of the aluminium into the metal substrate. Since it is known that silver [59] makes several intermetallic compounds with aluminium, the anodic

dissolution peaks could be ascribed to the aluminium from different intermetallic compounds, having naturally different dissolution potentials. This was confirmed by the GIXRD and EPMA analysis.

Alloying of silver with aluminium in the underpotential region becomes more pronounced with increasing melt temperature, indicating that diffusion of aluminium in the solid state becomes faster at higher temperatures.

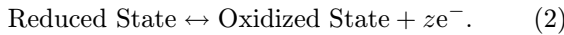
4.4. Calculation of Gibbs energy of formation from potential data

The equation correlating the equilibrium potential of a metal electrode and its ions in a solution was first derived by Nernst [60] and written in the general form that is applicable to electrodes of all types:

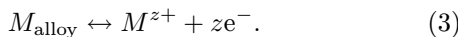
$$E = E^\circ + \frac{RT}{zF} \ln \frac{a_{\text{ox}}}{a_{\text{red}}}, \quad (1)$$

where a_{ox} and a_{red} are activities of the substances involved, R is the gas constant, T the absolute temperature, and F is Faraday's constant. The constant E° is the standard potential for the redox couple being considered (i.e. the potential measured when all the activities are equal to unity), the conditions being those corresponding to the standard state. Standard potentials are listed in most physical chemistry textbooks.

Equation (1) gives the potential of the electrode at which the reaction is:



Clearly, if the electrode is one consisting of an alloy containing metal M of valence z , reversible with respect to M^{z+} ions, so that the electrode reaction is:



The Nernst equation takes the form:

$$E_{M,\text{alloy}} = E_{M^{z+}/M}^\circ + \frac{RT}{zF} \ln \frac{a_{M^{z+}}}{a_{M,\text{alloy}}}, \quad (4)$$

where $a_{M,\text{alloy}}$ is the activity of the metal M in the alloy, $a_{M^{z+}}$ is activity of the M ions in the solution with which the alloy is in equilibrium.

The reversible potential of metal M in the solution, E_M , is given by:

$$E_M = E_{M^{z+}/M}^\circ + \frac{RT}{zF} \ln a_{M^{z+}}, \quad (5)$$

where $E_{M^{z+}/M}^\circ$ is the standard potential of metal M and $a_{M^{z+}}$ is the activity of M^{z+} ions in the solution; the activity of pure metal being taken as unity.

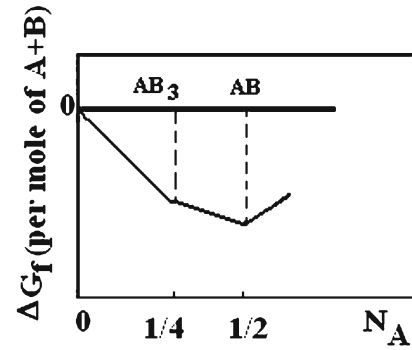


Fig. 6. Schematic diagram of free energy of formation against composition.

If the potential of an alloy is measured relative to a pure metal reference electrode, the potential measured is:

$$E_{M,\text{alloy}} - E_M = \frac{RT}{zF} \ln a_{M,\text{alloy}}. \quad (6)$$

It is this potential which is measured in the work described here (e.g., Fig. 2).

Formally, the activity of the metal M is defined in relation to the partial free energy of formation of the metal M in the alloy, thus:

$$RT \ln a = \Delta \bar{G}_A = \left(\frac{\partial \Delta G_{\text{f(ally)}}}{\partial N_A} \right). \quad (7)$$

Only in some cases is this activity simply related to the free energy of formation of an alloy or an intermetallic compound.

Consider a binary system AB_3 forming the intermediate stoichiometric compound AB and AB_3 .

The diagram of free-energy-of-formation (always per mole of $A + B$) against composition will look as shown in Fig. 6.

Between the stoichiometric compositions the total free energy of a given composition is simply a linear combination of the free energy of the two phases present ("lever rule" [61]).

Thus in the regions of this example the partial molar free energy of A :

$$\Delta \bar{G}_A = \left(\frac{d\Delta G_A}{dN_A} \right)_{T,P} \quad (8)$$

is constant between each of the compounds in the phase diagram, Fig. 7. Figure 7 represents a graphic form, which can be easily plotted using experimental values of the change in Nernstian overpotential with composition.

The general relation between the free energy of the system and the free energy of component A of a binary

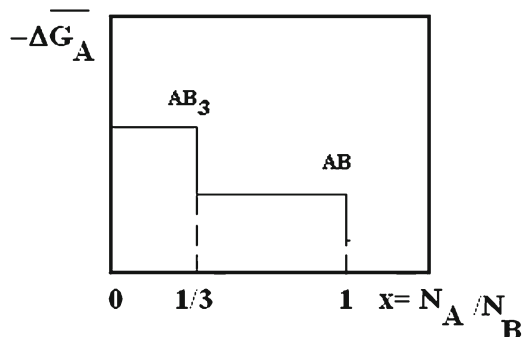


Fig. 7. Partial molar free energy of A as a function of molar ratio for the case where two stoichiometric intermetallic compounds, AB_3 and AB , are formed.

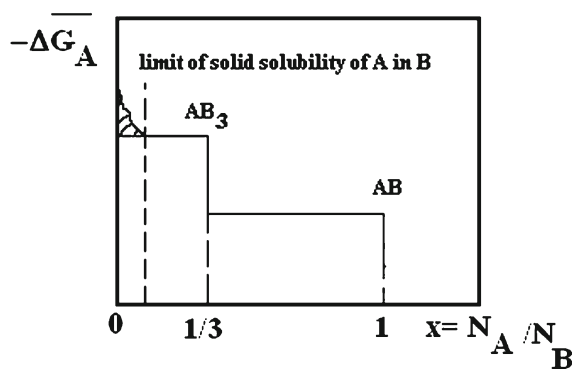


Fig. 8. Partial molar free energy of A as a function of molar ratio for the case where two stoichiometric compounds are formed and where there is a significant range of solubility of A in B .

system is given most conveniently by Duhem-Margules equation [62].

Within the first region of the phase diagram ($x = 0$ to $x = 1/3$) $\Delta\bar{G}_A$ is constant. In this case, the free energy value calculated from the Nernst equation corresponds to the free energy of formation, per mole of A , of the compound AB_3 . This simple result comes about because in this example, the energy needed to deposit the first atom of A in AB_3 is the same as the energy needed to deposit the last atom.

For the second intermediate compound, AB (as can be seen looking at Fig. 7) the integration of the Duhem-Margules equation must be carried out in two steps.

In general, to know the free energy of formation of any compound, it is necessary to have information not only on the partial free energy of A in that compound, but also in all the compounds (or solutions) which lie between the compound of interest and pure B . This has sometimes been omitted in literature.

If there is a significant range of solid solution of A in B , then this should also be taken into account.

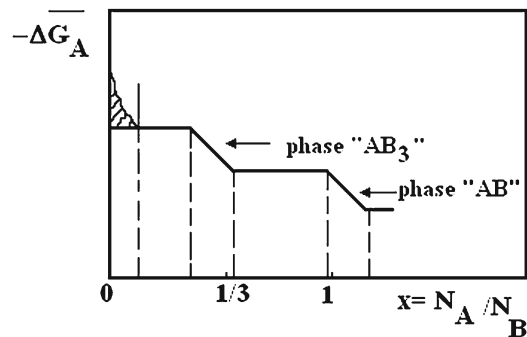


Fig. 9. Partial molar free energy of A as a function of molar ratio for the case where two compounds approximately AB and AB_3 with the range of stoichiometry are formed and where there is a significant range of solubility of A in B .

Figure 7 would then schematically appear as shown in Fig. 8.

The ratio of the shaded area to the total area under the curve represents the error involved in neglecting the solid solubility of A in B . Similarly, if the compounds also show a range of compositions, the schematic diagram given in Fig. 8 becomes as given in Fig. 9.

Here one can see that ΔG_f will depend somewhat on the exact composition of the compound. In practice, however, the range of stoichiometry is usually much smaller than the gaps in miscibility between one compound and the next; in this case it is more important to know the constant $\Delta\bar{G}_A$ values in the gaps than the change of $\Delta\bar{G}_A$ in the stoichiometric ranges. The error in ΔG_f will be of the same magnitude as its variation with stoichiometry.

It is important to note that although $\Delta\bar{G}_A$ (and ΔG_f) depend on the exact composition of the intermetallic compound, $\Delta\bar{G}_A$ is constant for mixtures of two adjacent compounds. This is shown by the flat sections of Fig. 7, which occur in the composition ranges associated with two co-existing phases. Thus, one can expect graphs of Nernstian overpotential against composition to show plateaux corresponding to each pair of co-existing phases.

The "open circuit" graphs provide probably the most accurate estimates of the reversible aluminium potential corresponding to pairs of phases on the metal surface. This is because they should not be influenced by the experimental conditions (e.g. scanning rate). Applying the Nernst equation to the potentials reported in Table 3 gives information on the partial molar Gibbs energy of aluminium existing on the surface at various times. This is constant when pairs of phases co-exist at the metal surface. In general, ΔG_f for a phase can only be calculated by Gibbs-Duhem integration [62]. To do this, a graph like Fig. 7 needs to be drawn, or at least visualized, based on the "open circuit" potential data. Following the proced-

Table 6. Average potential values of observed plateaux in “open circuit” measurements E , partial molar free energy of aluminium $\Delta\bar{G}_{\text{Al}}$ and free energies of formation ΔG_{f} of the assumed phases calculated at three different temperatures (* literature value [64])

t (°C)	200			250			300		
Phase composition	Plateau E (V vs. Al)	$\Delta\bar{G}_{\text{Al}}$ (kJ mol ⁻¹)	ΔG_{f} (kJ mol ⁻¹)	Plateau E (V vs. Al)	$\Delta\bar{G}_{\text{Al}}$ (kJ mol ⁻¹)	ΔG_{f} (kJ mol ⁻¹)	Plateau E (V vs. Al)	$\Delta\bar{G}_{\text{Al}}$ (kJ mol ⁻¹)	ΔG_{f} (kJ mol ⁻¹)
$\delta + \mu$ phase	0.11	-37.99	-43.53	0.12	-41.45	-47.50	0.11	-37.99	-43.53
μ phase + s.s. of Al and Ag	0.64	-185.3	-42.33 -29.3*	0.64	-185.3	-42.33 -29.7*	0.62	-185.3	-42.33 -30.2*
E_{rev} (V vs. Al)	0.92	-266.3		0.9	-260.5		0.87	-251.9	

ure in [63], one should construct a graph of the partial molar Gibbs energy of aluminium as a function of aluminium/silver mole ratio, and then integrate it up to the composition of interest.

The problem in the present case is that whereas one knows the potentials, and thus the values of the partial Gibbs energy of aluminium, $\Delta\bar{G}_{\text{Al}}$ corresponding to pairs of phases, one does not know ab initio, which phases or concentrations of aluminium these correspond to. This information can be surmised by matching the voltage plateaux to regions of the phase diagram where two phases co-exist. This procedure assumes that the phase diagram is obeyed. GIXRD and microanalysis data, which indicate which phases are actually present, can help in this matching.

According to silver-aluminium phase diagram [59] there are three two-phase regions at 250°C and 300°C:

- solid solution of Al in (Ag + μ) phase or Ag₃Al (12.5 to 21 at.% Al);
- ($\mu + \delta$) phase or Ag₂Al (24 to 33 at.% Al);
- δ phase + solid solution of Ag in Al (41.9 to 99.2 at.% Al).

It is obvious from Tables 3 and 4 that the number of plateaux observed in “open circuit” measurements in Fig. 2, as well as the number of phases identified by the GIXRD method, are less than the number of two-phase regions shown in Ag-Al phase diagram. At 200°C, 250°C and 300°C the plateau corresponding to Ag₂Al in equilibrium with (δ phase + solid solution in Al) is missing. Not surprising, because it seems unlikely that an Al solid solution containing only $\cong 0.5$ at.% of Ag could be formed at 0.01–0.150 V vs. Al.

The GIXRD data (Table 4) did not show all the phases [56–58], even if they showed plateaux in the electrochemical stripping or dissolution peaks in the anodic part of the LSV diagrams. Possible reasons might be: Ag-rich phases like (Ag₃Al) may be buried too deep for the X-rays to penetrate or some phases might be very thin because aluminium is too slow to diffuse in them.

However, at 250°C no plateaux are missing, so these data are used to assign phase pairs (Fig. 10).

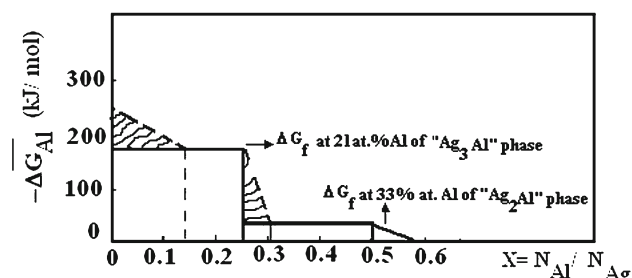


Fig. 10. Graphical representation of the calculation of (integral) free energies of formation ΔG_{f} from partial molar free energies calculated from “open circuit” plateau potentials. Data from Al in Ag at 250°C.

Then, for the other temperatures, it was assumed that the plateaux present corresponded to the ones at 250°C which occurred at similar potentials.

The calculated values of ΔG_{f} of the assumed phases are given in Table 6 together with partial molar Gibbs energy of aluminium and corresponding potential values of observed plateaux in the “open circuit” measurements at three different temperatures. In each case ΔG_{f} refers to the first phase of the quoted phase-pair (the one richer in aluminium, Table 4 and [56–58]), at its minimum-aluminium composition. No literature values for these data could be found for comparison: high temperature data cannot be extrapolated reliably because of the changes in the phase diagram.

A possible source of error is the assumed behaviour of $\Delta\bar{G}_{\text{Al}}$ as the mole fraction of aluminium approaches zero. The dashed line on Fig. 10 was drawn to the $\Delta\bar{G}_{\text{Al}}$ axis as implied by the measured open-circuit potential of silver in the electrolyte, even though in the theory the value of $\Delta\bar{G}_{\text{Al}}$ should asymptotically approach infinity at the axis.

4.5. The growth of layers of intermetallic compounds

The EPMA and X-ray results clearly show that successive layers of intermetallic compounds are for-

med at the surface of silver electrode. In order to interpret quantitatively the results of EPMA profiles, one needs a theory to describe the simultaneous growth of multiple layers of an intermetallic compound. In the literature one can find similar attempts [4, 12, 38, 40–43, 65, 66].

The Nernst equation is valid if the reaction is controlled by diffusion of aluminium into the substrate (and not by the activation rate control at the surface). This is demonstrated by the E - τ_d scans (“open circuit” stripping data): if the reaction was activation controlled, the rate of dissolution would get faster monotonically with increased overpotential. The plateaux observed show that it is sensitive to compound formation under the surface.

If rate control is by solid-state diffusion, then the surface reactions are in equilibrium, and since one applies a fixed potential, the Nernst equation predicts a fixed activity of aluminium on the surface. This is the diffusion boundary condition.

Surface and subsurface analysis shows more or less uniform layers on the surface so 1-D diffusion solution model is appropriate (i.e. no apparent problems of nucleation in the experimental time scale: restricted nucleation could give rise to three-dimensional growth of second phases).

4.5.1. Diffusion in solid solutions

Instead of the Fick equation:

$$J = -D \frac{dc}{dx}, \quad (9)$$

one may write [67]:

$$J = -ukTc \frac{d \ln a}{dx}, \quad (10)$$

where u is mobility, c is concentration, a is activity of the diffusing particles, k is Boltzmann’s constant, and T is absolute temperature.

Since in an ideal solution $a = c$, one could also use the Fick equation putting $D = ukT$.

In a non-ideal solution, one can use the activity coefficient γ (which is in general a function of c and $a = \gamma c$) and write:

$$J = -ukTc \frac{d \ln(\gamma c)}{dx}. \quad (11)$$

In a dilute Henrian solution, γ is constant, so one can say:

$$J = -ukT \frac{dc}{dx}, \quad (12)$$

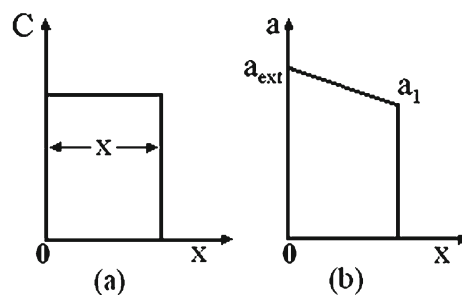


Fig. 11. The concentration gradient (a) and the corresponding activity gradient (b) for the case where one intermediate compound is formed.

which is simply Fick’s law and defines $D = ukT$ for any regular solution, including an ideal solution.

For non-regular solutions, Eq. (10) becomes:

$$J = -Dc \frac{d \ln a}{dx}. \quad (13)$$

4.5.2. Diffusion-limited growth of an intermetallic compound

Often it is possible to ignore the amount of aluminium in the substrate lattice by comparison to the large amount of aluminium in the surface compound. All diffusion is in the intermetallic compound.

The concentration gradient and the corresponding activity gradient can be presented as in Fig. 11(a) and (b), respectively.

Assuming the stoichiometry range of the compound is small, c is constant. Also one may assume u does not depend on stoichiometry; this is necessary since no information on how u varies with stoichiometry exists. Such an assumption is valid since the effects for an intermetallic compound will be much smaller than for ionic solids. Thus u will be an “average” mobility. There is no reaction between $x = 0$ and $x = x$, so J is constant. Thus after integration of Eq. (10) (for $x = 0$, $a = a_{\text{ext}}$; for $x = x$, $a = a_1$; and $a_1 < a_{\text{ext}}$):

$$J = cukT \frac{\ln a_{\text{ext}} - \ln a_1}{x}. \quad (14)$$

The rate of growth of the compound is given by:

$$\frac{dx}{d\tau} = J \frac{M}{f\rho}, \quad (15)$$

where M is the gram-atom mass of the compound, f is the atomic fraction of Al in compound, ρ is density of intermetallic compound and τ is time.

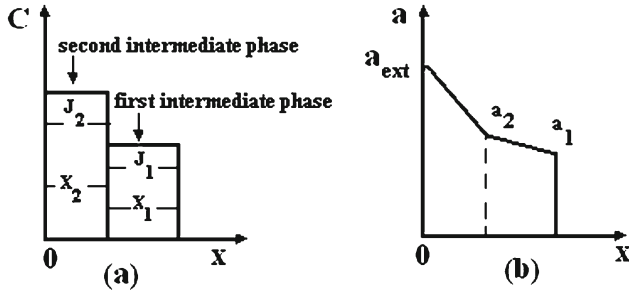


Fig. 12. Concentration gradients (a) and corresponding activity gradients (b) for the case where two intermediate compounds are formed.

Then from Eqs. (14) and (15) one obtains:

$$J = \frac{dx}{d\tau} \frac{f\rho}{M} = c_1 k T \frac{\ln a_{\text{ext}} - \ln a_1}{x}, \quad (16)$$

then:

$$\frac{x^2}{2} = \frac{M c_1 k T}{f\rho} (\ln a_{\text{ext}} - \ln a_1) \tau + \text{const.} \quad (17)$$

If $x = 0$ when $\tau = 0$ and $\text{const} = 0$:

$$x = \left[\frac{2 M c_1 k T}{f\rho} (\ln a_{\text{ext}} - \ln a_1) \tau \right]^{1/2}. \quad (18)$$

Thus one can see that $x \propto \tau^{1/2}$.

One can use the rule-of-thumb equation $x = \sqrt{2D\tau}$ and in this case the “diffusion coefficient” (better called a “thickening constant”) would be equal to:

$$“D” = \frac{M c_1 k T}{f\rho} (\ln a_{\text{ext}} - \ln a_1), \quad (19)$$

which is much different from the ideal $D = ukT$, and depends on the activity at the surface, and hence on the applied potential.

4.5.3. Diffusion with the formation of 2 intermediate compounds

The concentration gradients and the corresponding activity gradients have the form as shown in Fig. 12.

Using the same assumption as for a single phase, one has:

$$J_2 = c_2 k T u_2 \frac{(\ln a_{\text{ext}} - \ln a_2)}{x_2} \quad (20)$$

and:

$$J_1 = c_1 k T u_1 \frac{(\ln a_2 - \ln a_1)}{x_1}. \quad (21)$$

The rate of thickening of phase 2 is the rate of conversion of phase 1 into phase 2. Only aluminium arriving in flux J_2 and not diffusing on into phase 1 is available for the conversion. The volume converted for a given amount of aluminium is inversely proportional to the additional fraction of aluminium necessary to convert phase 1 into phase 2:

$$\frac{dx_2}{d\tau} = (J_2 - J_1) \frac{M_2}{\rho_2 (f_2 - f_1)}. \quad (22)$$

The rate of growth of phase 1 is the same as that for the single phase (Eq. (16)) except it is being consumed by phase 2, thus:

$$\frac{dx_1}{d\tau} = J_1 \frac{M_1}{f_1 \rho_1} - \frac{dx_2}{d\tau}. \quad (23)$$

Making the following abbreviations:

$$c_1 T k u_1 (\ln a_2 - \ln a_1) = C_1, \quad (24)$$

$$c_2 T k u_2 (\ln a_{\text{ext}} - \ln a_2) = C_2, \quad (25)$$

$$\frac{M_1}{f_1 \rho_1} = K_1, \quad (26)$$

$$\frac{M_2}{\rho_2 (f_2 - f_1)} = K_2, \quad (27)$$

and substituting Eqs. (20) and (21) into (22) gives:

$$\frac{dx_2}{d\tau} = \frac{K_2 C_2}{x_2} - \frac{K_2 C_1}{x_1}. \quad (28)$$

Similarly, substituting Eqs. (20) and (21) into (23) gives:

$$\frac{dx_1}{d\tau} = \frac{K_1 C_1}{x_1} - \frac{dx_2}{d\tau}. \quad (29)$$

Now, one can use a little intuition and try assuming that x_1 and x_2 still depend on $\sqrt{\tau}$:

$$x_1 = \sqrt{2A\tau} \text{ and } x_2 = \sqrt{2B\tau}, \quad (30)$$

where A and B are expressions to be determined. If they are independent of τ then the guess is correct.

Substituting x_1 and x_2 from Eq. (30) into Eqs. (28) and (29), multiplying the results by $\sqrt{2A\tau}$ and rearranging the obtained equation, one has:

$$\sqrt{B} = \frac{K_1 C_1}{\sqrt{A}} - \sqrt{A}. \quad (31)$$

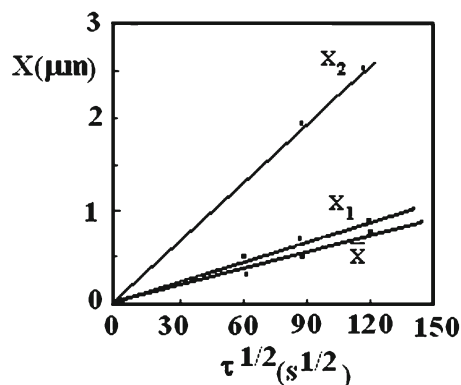


Fig. 13. Width of Al-rich layers formed on the surface of silver, as a function of square root of time: x_1 is the width of the inner layer of intermetallic compound, x_2 is the width of the outer intermetallic layer and \bar{x} is the width of a layer of pure Al which would contain the same total amount of Al.

It becomes obvious that both A and B are independent of time. In order for \sqrt{B} to be positive (and thus B to be real) the general “–” solution for A should be taken.

The final formula is complex, but the important point is that both layers increase their thickness proportionally to square root of time. The proportionality constant in the final formula ($x = \sqrt{2D\tau}$) for each layer is a complex function of the mobilities, densities, activity limits and compositions of both layers. The “ D ’s” are best called “thickening constants” to avoid the implication that they have a simple relation to the mobility, as in an ideal solution, Eq. (10). Note that the thickening constants for both layers depend on the activity applied at the surface, which is not predicted from the thoughtless application of the $x = \sqrt{2D\tau}$ approximation. The conclusions for the inner layer will apply also to further inner layers, if formed, since these will be mathematically identical to the single inner layer.

Figure 4 and data from Table 5 show how the thickness of the intermetallic layers, measured by EPMA, increases with time of UPD. According to the above-mentioned theory thickness of each intermetallic layer should increase with square root of time, under solid-state diffusion control. The points measured by EPMA usually showed one or more obvious steps corresponding to the compositions expected from the phase diagram and X-ray results.

The reasons why the steps are not better defined are:

- most phases show a range of compositions;
- the lateral resolution of the EPMA is of the order of 1 μm .

To arrive at the best estimate for the thickness of each layer, data from the phase diagram were used. In

Fig. 4 no clear steps are noticeable from the diagram and one can say that it is not possible to form a single phase in the composition ranges 12.5 to 21 at.% Al and 24 to 33 at.% Al. In these regions, one may draw vertical lines on the graph (in the other composition ranges the graph has a slight slope), because of the range in composition of the intermetallic phases. In this way one arrives at the reconstructed concentration profile shown with the corresponding widths of the layers (x_1 and x_2) of the two intermetallic compounds.

One can see that, given a lateral resolution of 1 μm for the EPMA, the measured points are just what one would expect for such a profile. The thicknesses of the inner (x_1) and outer (x_2) intermetallic layers formed on silver as a function of $\sqrt{\tau}$ are shown in Fig. 13 (data taken from the EPMA graphs such as in Fig. 4). The line (\bar{x}) on the graph corresponds to a “characteristic depth of aluminium penetration” defined in a way which allows comparison with the electrochemical stripping data. The thickness of x_2 layer obeys the theory well.

4.5.4. “Characteristic depth of aluminium penetration” and thickening of intermetallic layers as a function of time

According to the theory expounded above, the thickness of each intermetallic layer, including “buried” ones, should increase with square-root of time, under solid state diffusion control.

The charge of aluminium, $Q_{\text{Al},(\text{max})}$, dissolved from the Ag electrodes after Al underpotential deposition at different temperatures and different times obtained from linear sweep voltammograms is given in Table 2. These charges are time dependent and considerably higher than those corresponding to a close packed monolayer of aluminium, indicating the formation of an Al+Ag alloy in the region close to the interface. Figure 14 shows plots of $Q_{\text{Al},(\text{max})}$ as a function of $\tau_{\text{d}}^{1/2}$ obtained from anodic parts of voltammograms at various temperatures. Linear relationships are observed with intercepts at $\tau_{\text{d}} = 0$. Corresponding calculated slope ($\text{mC s}^{-1/2}$) for the curves in Fig. 14 is given in Table 7.

Under the assumption that the penetration depth (Δx) of the alloy into bulk metal can be estimated from the equation [66]:

$$\Delta x = \frac{MQ_{\text{a}}}{zF\rho}, \quad (32)$$

where $M = 26.98 \text{ g mol}^{-1}$ and $\rho = 2.38 \text{ g cm}^{-3}$ are the atomic mass and the density of aluminium, respectively, $z = 3$ is the charge involved per atom, and Q_{a} is the charge involved in formation of alloy after deposition at E_{d} for the time τ_{d} . Here Q_{a} is taken as the

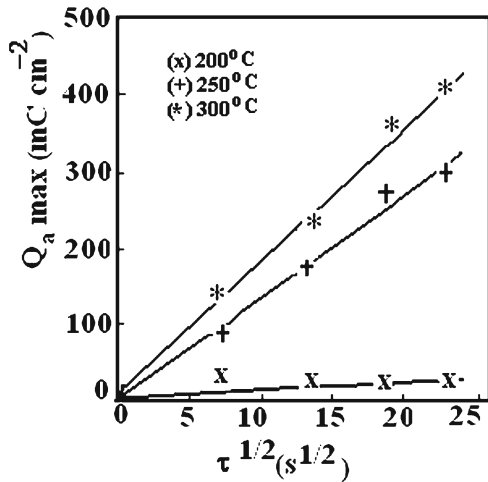


Fig. 14. Charge of aluminium dissolution $Q_{Al,(\max)}$ as a function of $\tau_d^{1/2}$ at 200°C, 250°C and 300°C for silver electrode.

Table 7. Calculated slopes ($\text{mC s}^{-1/2}$) for the curves in Fig. 16

Temperature (°C)	200	250	300
Calculated slope	1.01	12.9	16.9

Table 8. The “characteristic equivalent depth” of pure aluminium (μm) into silver electrode at different temperatures

Temperature (°C)	200	250	300
“Depth” (μm)	0.009	0.12	0.15

Table 9. Comparison of “overall diffusion coefficients” ($\text{cm}^2 \text{s}^{-1}$) for aluminium measured using electrochemical stripping and EPMA concentration profile

t (°C)	Stripping data	τ_d (h)	EPMA
200	7.8×10^{-16}	2	–
		1	1.7×10^{-13}
250	1.3×10^{-13}	2	1.9×10^{-13}
		4	1.9×10^{-13}
300	2.2×10^{-13}	2	6.0×10^{-13}

charge in excess of the value obtained from the extrapolation to τ_d , i.e. $Q_a = Q_{Al,(\max)} - Q_{Al,(\max),\tau_d=0}$. In fact this is thickness of an equivalent layer of pure aluminium, but it is difficult to make an easy cor-

rection for the density. In Table 8 the “characteristic depth of pure aluminium penetration” into silver electrode used is given in μm at different temperatures.

To get an overall D (obtained from LSV data), one needs to find the thickness of the layer of pure aluminium, which has the same amount of aluminium in it as the total amount diffused into the metal. It should be understood that this “characteristic depth of pure aluminium penetration” has little meaning in terms of the actual penetration of Al, but gives an indication of the amount of Al absorbed. From the “characteristic D ”, it is possible to estimate a sort of overall diffusion coefficient for aluminium in the substrates, using the well-known rule-of-thumb [68]:

$$(\Delta x)^2 = 2D\tau_d. \quad (33)$$

From Eqs. (32) and (33) it follows that a sort of overall diffusion coefficient of aluminium in the bulk of the metal (Ag) used is given by:

$$D = \frac{1}{2} \left(\frac{M}{zF\rho} \right)^2 \left(\frac{Q_a}{\sqrt{\tau_d}} \right)^2. \quad (34)$$

By taking $z = 3$, $M_{(Al)} = 26.98 \text{ g mol}^{-1}$ and $\rho_{(Al)} = 2.38 \text{ g cm}^{-3}$, calculated overall diffusion coefficients, “ D ”, of aluminium in the bulk of the metal used at three different temperatures are given in Table 9 under stripping data.

The “characteristic depth” obtained by EPMA also varies with $\sqrt{\tau}$, Fig. 13. Table 9 shows the “overall diffusion coefficient” calculated from characteristic depths (Eq. (33)), for each specimen examined with EPMA, compared to the values already reported from the stripping data. In general, agreement is good. The deviations tend to occur at the lower “ D ”, values, where errors in the measurements are more important. The EPMA values of “ D ” tend to be slightly higher, probably because of human tendency to measure the thickness of the layer where it is easiest, i.e., widest.

5. Conclusions

a) Electrochemical techniques used showed underpotential deposition of aluminium from equimolar $\text{AlCl}_3 + \text{NaCl}$ melt on silver substrate at temperatures ranging from 200°C to 300°C.

b) The UPD results in intermetallic compounds formation by solid-state diffusion of Al into the Ag substrate. Two intermetallic compounds could be distinguished: Ag_3Al {solid solution of Al in Ag + μ phase (12.5 to 21 at.% Al)} and Ag_2Al { $\mu + \delta$ phase (24 to 33 at.% Al)}. The results were consistent with established phase diagrams.

c) Linear dependence of the intermetallic layer thickness and the “characteristic aluminium penetration depth” on the square-root of deposition time was confirmed, both by EPMA analysis and by “open circuit” anodic stripping.

d) Thermodynamics shows that the constant potential regions measured during “open circuit” measurements correspond to the coexistence of pairs of intermetallic phases at the surface of silver.

e) The electrochemical potential of aluminium in a particular composition of the intermetallic compound can be converted directly to a free energy of formation, using the Nernst equation, only if no compounds or solution with lower concentration of Al can be formed. In general, a Gibbs-Duhem integration must be performed to arrive at free energies of formation from measured electrode potentials.

References

- [1] BRENNER, A.: *Electrodeposition of Alloys*. Vol. 1. New York, Academic Press 1963.
- [2] GORBUNOVA, K. M.—POLUKAROV, Y. M.: In: *Advances in Electrochemistry and Electrochemical Engineering*. Ed.: Tobias, C. W. New York, Wiley 1967, p. 249.
- [3] DESPIĆ, A. R.—JOVIĆ, V. D.: In: *Modern Aspects of Electrochemistry*. Ed.: White, R. E. New York, Plenum Press 1995, p. 143.
- [4] BUDEVSKI, E.—STAIKOV, G.—LORENZ, W. J.: *Electrochemical Phase Formation and Growth*. Weinheim, VCH 1996.
- [5] SMITH, W. F.: *Structures and Properties of Engineering Alloys*. New York, McGraw Hill Book Company 1981.
- [6] SCORDILIS-KELLEY, C.—FUULLER, J.—CARLIN, R. T.: *J. Electrochem. Soc.*, 139, 1992, p. 694.
- [7] STAFFORD, G. R.—JOVIĆ, V. D.—HUSSEY, C. L.: *Materials Science Forum*, 352, 2000, p. 49.
- [8] TSUDA, T.—HUSSEY, C. L.—STAFFORD, G. R.: *J. Electrochem. Soc.*, 152, 2005.
- [9] CHEN, P.-YU.—HUSSEY, C. L.: *Electrochim. Acta*, 52, 2007, p. 1857.
- [10] AUSTIN, L. W.—VUCICH, M. G.—SMITH, E. J.: *J. Electrochem. Tech.*, 1, 1963, p. 267.
- [11] DELIMARSKII, Y. K.—MAKOGON, V. F.—KUZMOVICH, V. V.: *Zashch. Metal.*, 4, 1968, p. 743.
- [12] STAFFORD, G. R.—HUSSEY, C. L.: In: *Advances in Electrochemical Science and Engineering*. Vol. 7. Eds.: Alkire, R. C., Kolb, D. M. Weinheim, Wiley-VCH Verlag GmbH 2001.
- [13] MAMANTOV, G.—HUSSEY, C. L.—MARASSI, R.: In: *Techniques for Characterisation of Electrodes and Electrochemical Processes*. Eds.: Varma, R., Selman, J. R. New York, Wiley 1991, p. 471.
- [14] JOVIĆ, V. D.—JOVIĆEVIĆ, J. N.: *J. Appl. Electrochemistry*, 19, 1989, p. 275.
- [15] JAFARIAN, M.—GOBAL, F.—DANAEE, I.—MAHJANI, M. G.: *Electrochim. Acta*, 52, 2007, p. 5437.
- [16] STAFFORD, G. R.—HAARBERG, G. M.: *Plasmas and Ions*, 1, 1999, p. 35.
- [17] UEDA, M.—KIGAWA, H.—OHTSUDA, T.: *Electrochim. Acta*, 52, 2007, p. 2515.
- [18] TIERNEY, B. J.—PITNER, W. R.—MITCHELL, J. A.—HUSSEY, C. L.—STAFFORD, G. R.: *J. Electrochem. Soc.*, 145, 1998, p. 3110.
- [19] CARLIN, R. T.—WILKES, J. S.: In: *Chemistry of Nonaqueous Solutions*. Eds.: Mamantov, G., Popov, A. I. New York, VCH Publishers 1994, p. 277.
- [20] ABBOT, A. P.—McKENZIE, K. J.: *Phys. Chem. Chem. Phys.*, 8, 2006, p. 4265.
- [21] GEETHA, S.—TRIVEDI, D. C.: *Bulletin of Electrochemistry*, 19, 2003, p. 37.
- [22] HUSSEY, C. L.: In: *Electroanalytical Chemistry in Molten Salts*. Eds.: Kissinger, P. T., Heinmann, W. R. New York, Marcel Dekker 1996, p. 511.
- [23] KOLB, D. M.: In: *Advances in Electrochemistry and Electrochemical Engineering*. Eds.: Gerischer, H., Tobias, C. W. New York, Wiley 1978, p. 125.
- [24] KOLB, D. M.: In: *Advances in Electrochemical Science and Engineering*. Vol. 7. Eds.: Alkire, R. C., Kolb, D. M. Weinheim, Wiley-VCH 2001.
- [25] BEWICK, A.—JOVIĆEVIĆ, J. N.—THOMAS, B.: *Faraday Symposia of the Chem. Soc.*, 12, 1977, p. 24.
- [26] JOVIĆ, V. D.—JOVIĆEVIĆ, J. N.—DESPIĆ, A. R.: In: *Zbornik referatov 8. Jugoslovenski Simposij o Elektrokemiji*, Dubrovnik. Ed.: Dolar, D. Katedra za Fizikalno kemijo, Univerze E. Kardelja v Ljubljani 1983, p. 151.
- [27] JOVIĆEVIĆ, J. N.—JOVIĆ, V. D.—DESPIĆ, A. R.: *Electrochim. Acta*, 29, 1984, p. 1625.
- [28] JOVIĆ, V. D.—JOVIĆEVIĆ, J. N.: *Electrochim. Acta*, 30, 1985, p. 1455.
- [29] JOVIĆEVIĆ, J. N.—BEWICK, A.: *Facta Universitatis, Series Physics, Chemistry and Technology*, 3/2, 2005, p. 183.
- [30] THAMBIDURAI, C.—KIM, Y.-G.—STICKNEY, J. L.: *Electrochim. Acta*, 53, 2008, p. 6157.
- [31] HUANG, J. F.—SUN, I. W.: *J. Electrochem. Soc.*, 149, 2002, p. E348.
- [32] HSIU, S. I.—TAI, C. C.—SUN, I. W.: *Electrochim. Acta*, 51, 2006, p. 2607.
- [33] RADOVIĆ, B. S.: *The Growth and Characterization of Novel Al Surface Coatings Prepared by Underpotential Deposition from Low Temperature Melts*. [PhD Thesis]. University of Strathclyde 1992.
- [34] RADOVIĆ, B. S.—EDWARDS, R. A. H.—JOVIĆEVIĆ, J. N.: *J. Electroanal. Chem.*, 428, 1997, p. 113.
- [35] JOVIĆ, V. D.: *J. Serb. Chem. Soc.*, 71, 2006, p. 373.
- [36] JOHNSTON, M.—LEE, J.-JOON.—CHOTTINER, G. S.—MILLER, B.—TSUDA, T.—HUSSEY, C. L.—SCHERSON, D. A.: *J. Phys. Chem. B*, 109, 2005, p. 11296.
- [37] STAFFORD, G. R.—KONGSTEIN, O. E.—HAARBERG, G. M.: *J. Electrochem. Soc.*, 153, 2006, p. C207.
- [38] BORT, H.—JUTTNER, K.—LORENZ, W.—STAIKOV, G.: *Electrochim. Acta*, 28, 1983, p. 993.
- [39] BONDOS, J. C.—GEWIRTH, A. A.—NUZZO, R. G.: *J. Phys. Chem.*, 100, 1996, p. 8617.
- [40] VIDU, R.—HARA, S.: *J. Electroanal. Chem.*, 475, 1999, p. 171.
- [41] VIDU, R.—HARA, S.: *Surface Sci.*, 452, 2000, p. 229.
- [42] VIDU, R.—HIRAI, N.—HARA, S.: *Phys. Chem.*

- Chem. Phys., 3, 2001, p. 3320.
- [43] GARCIA, S. G.—SALINAS, D. R.—STAIKOV, G.: *Surface Sci.*, 57, 2005, p. 9.
- [44] ZELL, C. A.—ENDRES, F.—FREYLAND, W.: *Phys. Chem. Chem. Phys.*, 1, 1999, p. 697.
- [45] MORIMITSU, M.—TANAKA, N.—MATSUNAGA, M.: *Molten Salts XIII*, 19, 2002, p. 671.
- [46] ZHU, Q.—HUSSEY, C. L.—STAFFORD, G. R.: *J. Electrochem. Soc.*, 148, 2001, p. C88.
- [47] YAN, Y. D.—ZHANG, M. L.—HUE, Y.—HAN, W.—CAO, D. X.—HE, L. Y.: *J. Appl. Electrochemistry*, 39, 2009, p. 455.
- [48] ABBOT, A. P.—EARDLEY, C. A.—FARLEY, N. R.—GRIFFITH, G. A.—PRATT, A.: *J. Appl. Electrochemistry*, 31, 2001, p. 1345.
- [49] ZELL, C. A.—FREYLAND, W.: *Chemical Physics Letters*, 337, 2001, p. 293.
- [50] FORNI, F.—INNOCENTI, M.—PEZZATINI, G.—FORESTI, M. L.: *Electrochim. Acta*, 45, 2000, p. 3225.
- [51] BOUROUSHIAN, M.—KOSANOVIC, T.—LOIZOS, Z.—SPYRELLIS, N.: *Electrochemistry Communications*, 2, 2000, p. 281.
- [52] CAVALLOTTI, P. L.—NOBILI, L.—VICENZO, A.: *Electrochim. Acta*, 50, 2005, p. 4557.
- [53] LEE, J. J.—BAE, I. T.—SCHERSON, D. A.—MILLER, B.—WHEELER, K. A.: *J. Electrochem. Soc.*, 147, 2000, p. 562.
- [54] KIM, J. Y.—KIM, Y.—GEUN.—STICKNEY, J. L.: *Journal of Electroanalytical Chemistry*, 621, 2008, p. 205.
- [55] GREELEY, J.—NORSKOV, J. K.: *Electrochim. Acta*, 52, 2007, p. 5829.
- [56] Joint Committee on Powder Diffraction Standards, *Powder Diffraction File* 14-674.
- [57] Joint Committee on Powder Diffraction Standards, *Powder Diffraction File* 4-0783.
- [58] Joint Committee on Powder Diffraction Standards, *Powder Diffraction File* 26-1330.
- [59] McALISTER, A. J.: *Bull. Alloy Phase Diagrams*, 8, 1987, p. 526.
- [60] NERNST, W.: *Z. Phys. Chem.*, 4, 1889, p. 129.
- [61] CAHN, R. W.: *Physical Metallurgy*. Amsterdam, North-Holland Publishing Company, 1970.
- [62] KUBASCHEWSKI, O.—EVANS, E. L.: *Metallurgical Thermochemistry*. London, Pergamon 1958.
- [63] DARKEN, L. S.—GURRY, R. W.: *Physical Chemistry of Metals*. New York, McGraw-Hill 1953.
- [64] STULL, D. R.—PROPHET, H.: *JANAF Thermochemical Tables*. Washington, D.C., National Bureau of Standards, Publication 37, 1971.
- [65] MOFFAT, T. P.: *J. Electrochem. Soc.*, 141, 1994, p. 3059.
- [66] SALVAREZZA, R. C.—VASQUEZMOLL, D. V.—GIORDANO, M. C.—ARVIA, A. J.: *J. Electroanal. Chem.*, 213, 1986, p. 301.
- [67] JOST, W.: *Diffusion*. New York, Academic Press 1952.
- [68] ATKINS, P. W.: *Physical Chemistry*. San Francisco, Freeman 1982.